https://doi.org/10.5194/essd-2026-426
Preprint. Discussion started: 19 June 2026

Open Access Earth System Science Data Discussions

Extending Daily River Discharge Records Across China Using Satellite-Derived River Widths

Yong Wang[1], Yulin Gong[1], Yinghong Jing[1], Xiaojun She[1], Yao Li[1,*]

[1]School of Geographical Sciences, Southwest University, Chongqing 400715, China.

Corresponding author: Yao Li (liyao7@swu.edu.cn)

Abstract. Long-term monitoring of global river discharge has been hindered by the uneven distribution of gauging stations and limited data accessibility, a challenge that is particularly acute in China. Although China contains one of the world's densest river networks, high-frequency in situ discharge observations remain largely unavailable in the international public domain. To address this gap, we compiled daily discharge records from 1,196 gauges across China, comprising approximately 2.33 million observations—39 times as many gauges as are currently available for the region in the Global Runoff Data Centre (GRDC). Leveraging this unprecedented collection of in situ discharge records, along with river width time series derived from Landsat and Sentinel-2 imagery and gauge-specific hydraulic geometry relationships, we reconstructed and extended daily river discharge observations for 310 gauges from 1990 to 2024, resulting in the China Daily River Discharge Records (CDR^2) dataset. Compared with existing global satellite-derived discharge products, CDR^2 increases the number of available gauges in China by at least fivefold. It achieves substantially improved performance, with a median Kling–Gupta efficiency of 0.66 during validation. Sensitivity analyses further indicate that discharge estimation accuracy increases markedly with greater river width variability and stronger hydraulic sensitivity. Trend analysis reveals that nearly 65% of gauges exhibit declining discharge over 1990–2024, with a median relative trend of −0.21%/yr, most pronounced in the Haihe, Liaohe, Yellow River, and middle Yangtze River basins. As the most extensive satellite-derived, gauge-constrained daily discharge dataset currently available for China, CDR^2 bridges a critical geographic gap in global river monitoring and provides a valuable benchmark for future discharge estimation, hydrological studies, and satellite calibration efforts.

Keywords: river discharge; river width; satellite remote sensing; hydraulic geometry; China.

https://doi.org/10.5194/essd-2026-426
Preprint. Discussion started: 19 June 2026

Open Access Earth System Science Data Discussions

1 Introduction

Despite accounting for only a small fraction of the global freshwater inventory, rivers constitute one of the most dynamic components of the hydrological cycle (Oki and Kanae, 2006; Palmer and Ruhi, 2018). They not only provide the most accessible freshwater resource for human societies but also serve as critical biogeochemical conduits linking terrestrial and marine ecosystems through the transport of sediments, nutrients, and thermal energy (Syvitski et al., 2005; Allen and Pavelsky, 2018; Resplandy et al., 2018). Consequently, the accurate and continuous quantification of river discharge is fundamental for sustainable water resource management, reliable hydroclimatic modeling, and assessments of environmental change.

Traditionally, in situ gauging networks have served as the primary benchmark for river discharge monitoring, providing high-fidelity and temporally continuous observations (Alsdorf et al., 2007; Hannah et al., 2011; Andrews and Grantham, 2024). However, the global distribution of these networks is highly uneven. While North America and Europe maintain relatively dense monitoring systems, extensive regions across Asia, Africa, and South America remain poorly gauged or entirely data-sparse (Do et al., 2018; Krabbenhoft et al., 2022; Collins et al., 2024; Oh and Bartos, 2025; Sun et al., 2026). Moreover, even where gauging infrastructure exists, the access to discharge records is often restricted by geopolitical barriers and limited data-sharing policies (Fekete et al., 2015; Famiglietti et al., 2015; Ruhi et al., 2018; Collins et al., 2024). Together, these limitations substantially hinder the global characterization of fluvial dynamics and have motivated the rapid development of satellite-based Earth observation and hydrological modeling approaches to address observational gaps (Gleason et al., 2014; Lin et al., 2019; Ghiggi et al., 2019; Hao et al., 2024; Scherer et al., 2024).

Hydrological models can provide spatially and temporally continuous simulations of river discharge, yet their predictive accuracy remains constrained by uncertainties in meteorological forcing data and simplified representations of hydrological processes (Beven, 2007; Zheng et al., 2019; Tang et al., 2023). In contrast, satellite remote sensing has emerged as a promising alternative, owing to its unprecedented global coverage and continually improving spatiotemporal resolutions (Lettenmaier et al., 2015; Sichangi et al., 2017; Hou et al., 2020). Although satellites cannot directly measure river discharge, they can routinely retrieve key hydraulic variables such as water surface elevation, river width, and surface slope (Smith et al., 1997; Bonnema et al., 2016; Durand et al., 2016). When integrated with historical in situ measurements, these remotely sensed

https://doi.org/10.5194/essd-2026-426
Preprint. Discussion started: 19 June 2026

variables can be converted into continuous discharge estimates using empirical hydraulic geometry relationships and rating-based approaches (Pavelsky, 2014; Paris et al., 2016). Conceptually, this framework parallels conventional stage–discharge rating curves employed at gauging stations, with satellite-derived river width or water surface elevation replacing ground-based stage measurements.

In recent years, satellite earth observations have facilitated substantial progress in extending global river discharge records. Notably, the Satellite Altimetry-based Extension of global-scale in situ river discharge Measurements (SAEM) integrated multi-mission satellite altimetry with existing stream gauging networks to reconstruct discharge at 8,730 global stations, representing approximately 88% of the globally gauged discharge volume (Saemian et al., 2024). Meanwhile, optical remote sensing has demonstrated strong capability for width-based discharge estimation. Riggs et al. (2023) utilized Landsat and Sentinel-2 imagery to extract dynamic river widths and extended discharge records for 2,168 gauges globally. Similarly, Lin et al. (2023) conducted a large-sample evaluation of width-based discharge algorithms across 3,078 gauges, demonstrating their scalability and sensitivity to hydraulic and geomorphological conditions. More recently, multi-sensor integration has emerged as a promising strategy to maximize observational coverage and reliability. Elmi et al. (2024) combined satellite-derived river widths with altimetry-based water levels and applied a stochastic non-parametric framework to reconstruct monthly discharge time series for 3,377 discontinued Global Runoff Data Centre (GRDC) stations, resulting in the Remote Sensing-based Extension for the GRDC (RSEG) dataset with rigorous uncertainty quantification.

Despite these substantial global advances, a critical geographic gap persists in China. China hosts one of the world's largest and most diverse river systems and is undergoing profound hydrological alterations. River discharge regimes across the country are increasingly shaped by the combined influences of climate change—including accelerated glacier retreat over the Tibetan Plateau—and intensified anthropogenic regulation such as land use change and reservoir operation (Yao et al., 2022; Yang et al., 2022; Wang et al., 2025a; Wang et al., 2025b). Nevertheless, due to restrictive data-sharing policies, high-frequency in situ discharge observations from China remain largely inaccessible. This scarcity is particularly evident in the GRDC, the most comprehensive global archive of river discharge observations, which currently contains records for only 31 gauges within China (Färber et al., 2025). In addition, China is severely underrepresented in existing

https://doi.org/10.5194/essd-2026-426
Preprint. Discussion started: 19 June 2026

global remote sensing discharge products. For example, the SAEM dataset encompasses only 62 gauges across China, accounting for less than 1% of its total reconstructed gauges (Saemian et al., 2024). This stark disparity underscores a major deficiency in the global characterization of river discharge dynamics across one of the world's most hydrologically important regions.

To address this gap, this study leverages river width observations derived from Landsat and Sentinel optical imagery to establish station-specific width–discharge relationships and reconstruct daily river discharge records for 310 gauges across China. To our knowledge, this represents the most comprehensive satellite-derived discharge reconstruction for China to date. Compared with existing global datasets, the number of gauge-constrained stations within China has increased by at least fivefold. Across all validation gauges, the reconstructed discharge achieves a median Kling–Gupta Efficiency (KGE) of 0.66, outperforming currently available global products. The resulting dataset, termed the China Daily River Discharge Records (CDR^2), substantially expands long-term discharge observations in a hydrologically critical yet data-sparse region. Beyond improving regional hydrological monitoring, CDR^2 provides an essential benchmark for assessing riverine responses to climate change and anthropogenic disturbances and contributes valuable observations for future global hydrological modeling and satellite calibration efforts.

2 Data and Methods

This section describes the datasets, remote sensing products, and methodological framework used to reconstruct and extend river discharge observations across China. The workflow integrates in situ discharge measurements, satellite-derived river width observations from Landsat and Sentinel-2 imagery, and station-specific hydraulic geometry relationships to generate continuous daily discharge records. Fig. 1 provides an overview of the technical framework, including data acquisition, river width extraction, construction of width–discharge relationships, discharge reconstruction, and validation procedures. Detailed descriptions of the datasets, preprocessing steps, and reconstruction methods are presented in the following subsections.

https://doi.org/10.5194/essd-2026-426
Preprint. Discussion started: 19 June 2026

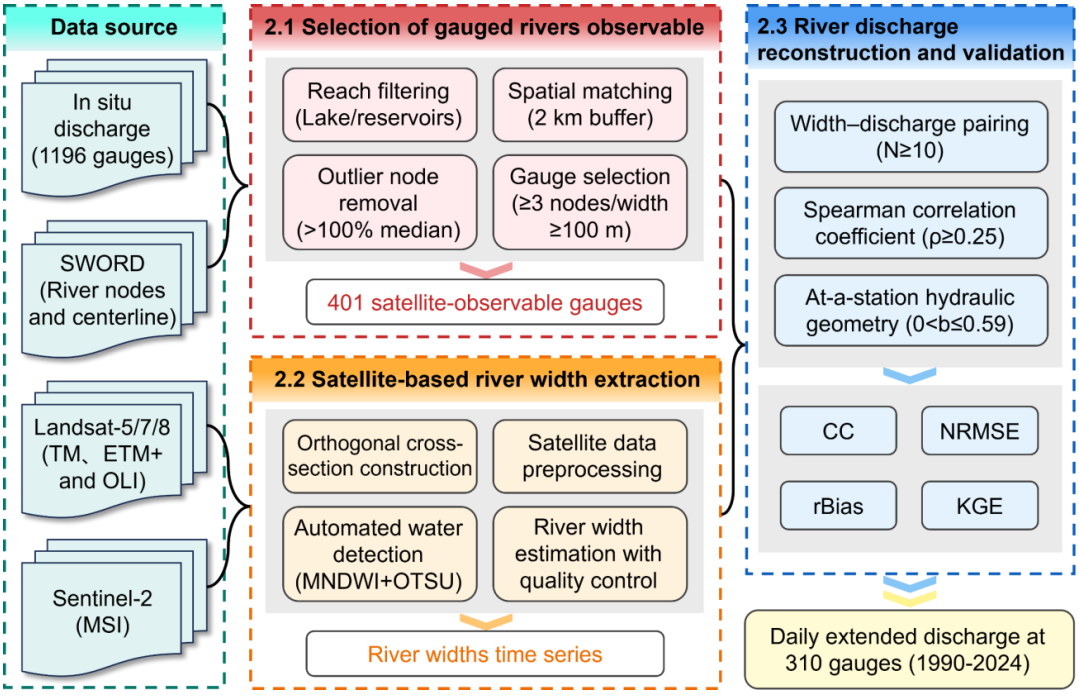

Figure 1. Technical framework of the study.

2.1 Selection of gauged rivers observable

Daily in situ river discharge observations were obtained from the National Hydrological and Rainfall Information System of the Ministry of Water Resources of China, which integrates national and provincial monitoring networks spanning major rivers, lakes, and reservoirs and provides real-time and historical records of water level, discharge, and storage. We compiled daily discharge records from 1,196 gauging stations across 2014–2024 to construct the CDR^2 dataset (Fig. 2a). To minimize redundancy, when multiple gauges were located within 100 m of one another, only the station with the longest observational record was retained. The resulting gauge network spans nearly all major river basins in China, except the Southwest River Basin. Mean discharge among the selected gauges ranges from 0.5 to 30,000 m^3/s, with each station containing an average of 1,945 observations. In terms of temporal coverage, more than 80% of the gauges contain observations beginning in or before 2015, while over 90% include records extending back to 2018 or earlier (Fig. 2c). Collectively, these characteristics demonstrate that CDR^2 provides

https://doi.org/10.5194/essd-2026-426
Preprint. Discussion started: 19 June 2026

both extensive spatial coverage and high-frequency discharge observations across China, offering a valuable foundation for large-scale hydrological reconstruction and analysis.

Compared with existing publicly available global discharge datasets, CDR^2 substantially improves both the spatial coverage and observational availability of river discharge records across China. The GRDC, currently the most comprehensive global archive of in situ discharge observations, contains records from only 31 gauges in China, many of which predate 2004 and have relatively short observational periods, including some with only a single year of data. Similarly, the Chinese Hydrology Project (CHP) dataset provides discharge records from 141 gauges, primarily spanning 1953–1987 (Henck et al., 2010; Schmidt et al., 2011). In contrast, CDR^2 incorporates approximately 8.5 times as many gauges as CHP and 38.6 times as many as GRDC (Fig. 2d), while also offering substantially more recent observations at a daily temporal resolution.

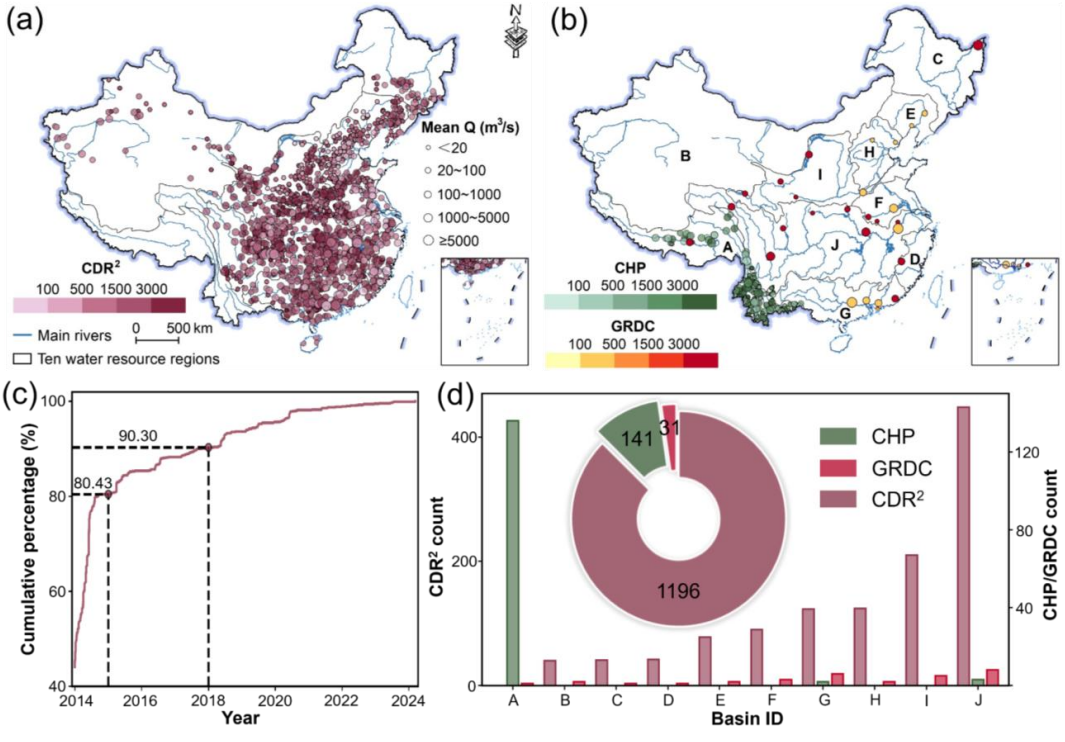

Figure 2. Spatial distribution and temporal coverage of in situ river discharge observations across China (2014–2024). (**a**) Spatial distribution of the 1,196 gauges included in the China Daily River Discharge Records (CDR^2) dataset, with symbol size representing mean discharge (Q, m³/s). (**b**) Spatial distribution of river gauges available from the Chinese Hydrology Project (CHP) and the

https://doi.org/10.5194/essd-2026-426
Preprint. Discussion started: 19 June 2026

148 Global Runoff Data Centre (GRDC) within China. The labeled regions (A–J) denote the ten major
149 basins: Southwest Rivers (A), Northwest Rivers (B), Songhua River (C), Southeast Rivers (D),
150 Liao River (E), Hai River (F), Pearl River (G), Huai River (H), Yellow River (I), and Yangtze
151 River (J). (**c**) Cumulative probability distribution of gauge observation start years in the CDR^2,
152 indicating that over 80% of gauges contain records beginning in or before 2015, while more than
153 90% begin in or before 2018. **(d)** Comparison of the number of gauges included in the CDR^2, CHP,
154 and GRDC datasets across China.

155 To identify gauges suitable for satellite-based discharge reconstruction, we employed the
156 Surface Water and Ocean Topography River Database (SWORD) (Altenau et al., 2021) as the
157 reference river network. SWORD provides a globally consistent river centerline dataset with
158 connected topology, in which river systems are segmented into predefined reaches and nodes. To
159 minimize the influence of non-channel water bodies, river reaches linked to lakes and reservoirs
160 were excluded using the SWORD lakeflag attribute. For each gauge, all river nodes located within
161 a 2 km buffer radius were extracted to establish the spatial correspondence between in situ
162 discharge observations and satellite-observed river width. To improve robustness, outlier nodes
163 were removed using a median-based relative deviation criterion, whereby nodes with width
164 deviations exceeding 100% of the median width were considered anomalous and excluded. A
165 gauge was retained only if it satisfied two conditions: (1) the presence of at least three valid
166 matched nodes, and (2) at least one node with a mean river width of ≥100 m, as defined in SWORD.
167 These criteria ensured that the river channel could be reliably detected by optical satellite imagery
168 and that the extracted width measurements were sufficiently representative for discharge
169 reconstruction. Following the screening procedure, 401 gauges were identified as suitable for
170 satellite-based analysis (Fig. 3). The mean discharge of these gauges ranges from 1.66 to 27,797.46
171 m^3/s, with a median of 217 m^3/s and a mean of 1,090 m^3/s. The corresponding river widths range
172 from 69 to 3,504 m, with a median of 191 m and a mean of 277 m.

https://doi.org/10.5194/essd-2026-426
Preprint. Discussion started: 19 June 2026

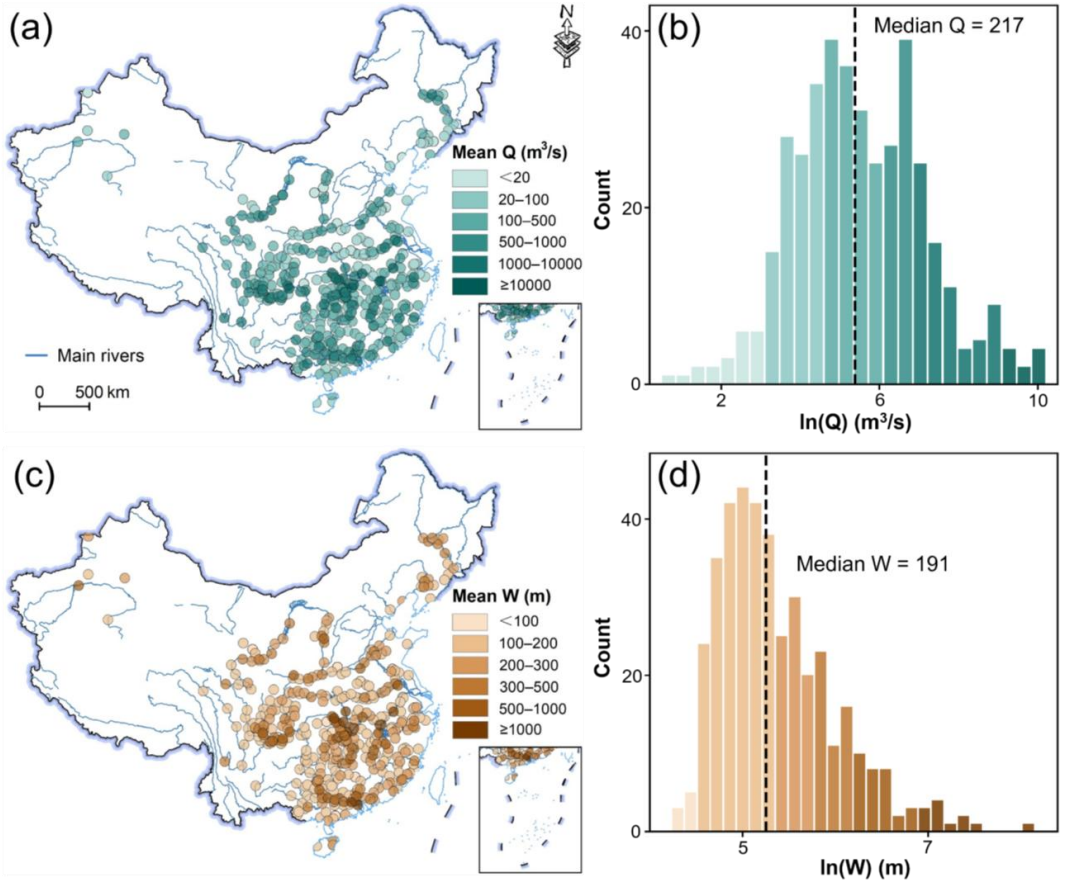

Figure 3. Spatial distribution and hydrological characteristics of gauges selected for satellite-based discharge reconstruction. (**a**) Spatial distribution of the 401 selected gauges, with symbol color representing mean discharge (Q, m³/s). (**b**) Frequency distribution of ln(Q) for the selected gauges, showing a median discharge of 217 m³/s. (**c**) Spatial distribution of the corresponding mean river width (W, m) for the selected gauges. (**d**) Frequency distribution of ln(W), with a median river width of 191 m.

2.2 Satellite-based river width extraction

2.2.1 Construction of orthogonal river cross-sections

To retrieve long-term river width time series, we implemented an automated fixed-geometry approach based on predefined orthogonal cross-sections (Fig. 4). Unlike approaches that dynamically determine cross-section orientation for each individual image, the orthogonal

https://doi.org/10.5194/essd-2026-426
Preprint. Discussion started: 19 June 2026

Open Access Earth System Science Data Discussions

directions in this study were derived once from the river centerline and consistently applied throughout the entire satellite image archive, thereby substantially improving computational efficiency (Pavelsky and Smith, 2008; Yang et al., 2019; Feng et al., 2019). For each matched river node identified in Section 2.1, its location was projected onto the river centerline to determine its along-channel position. Local flow direction was then estimated using two control points sampled symmetrically upstream and downstream along the centerline. To ensure directional stability across rivers of varying sizes, the sampling distance was constrained to 1–10 m. The resulting tangent vector was normalized and rotated by 90° to derive the unit normal vector perpendicular to the local flow direction. Orthogonal cross-sections were centered at the projected node location and extended 1.5$\bar{W}$ on both sides of the channel centerline, where $\bar{W}$ represents the prior mean river width derived from SWORD, yielding a total transect length of 3$\bar{W}$. This proportional design ensures full coverage of the active river channel while minimizing contamination from adjacent floodplains, wetlands, or nearby water bodies. In cases where local centerline curvature or geometric discontinuities prevented reliable tangent estimation, the orthogonal cross-sections were defined using the perpendicular direction of the nearest valid centerline segment.

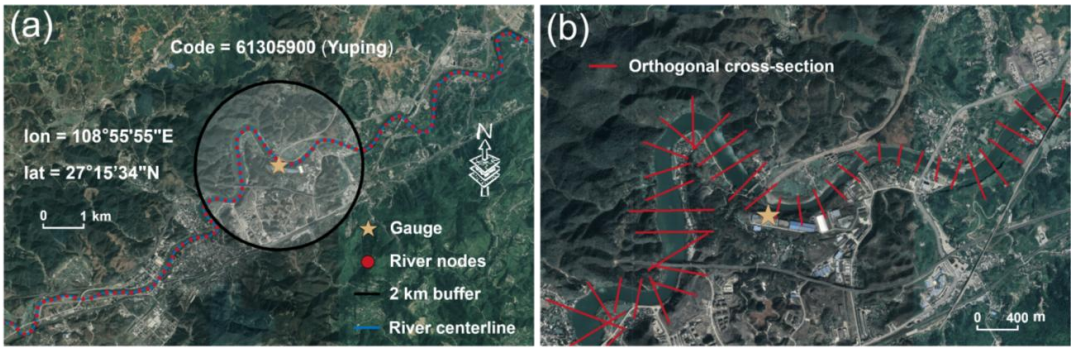

Figure 4. Construction of orthogonal cross-sections for satellite-based river width extraction. (**a**) Example at the Yuping gauge illustrating the gauge location, river centerline, and associated river nodes. (**b**) Orthogonal cross-sections generated at each river node along the river centerline for extracting river width from satellite imagery. Source of the underlying image: © Google Earth.

2.2.2 Satellite data preprocessing and surface water detection

River width was derived from optical satellite imagery acquired from Landsat-5/7/8 and Sentinel-2 during 1990–2024 and processed on the Google Earth Engine (GEE) cloud platform (Table 1). Level-2 surface reflectance products were employed to ensure radiometric consistency

https://doi.org/10.5194/essd-2026-426
Preprint. Discussion started: 19 June 2026

and accurate geolocation across sensors. To mitigate the effects of cloud contamination, images with scene-level cloud cover exceeding 25% were excluded. Additional pixel-level masking was applied using sensor-specific quality assessment (QA) bands to remove clouds, cloud shadows, and cirrus contamination. For days with multiple valid observations, median compositing was performed to generate daily surface reflectance mosaics with reduced cloud-related noise. Water bodies were identified using the Modified Normalized Difference Water Index (MNDWI) (Xu, 2006), calculated as:

$$\mathrm{MNDWI} = \frac{\mathrm{Green}-\mathrm{SWIR}}{\mathrm{Green}+\mathrm{SWIR}} \quad (1)$$

Compared with the traditional Normalized Difference Water Index (NDWI) (McFeeters, 1996), MNDWI more effectively suppresses signals from built-up land surfaces and improves the delineation of open water bodies. Binary water masks were subsequently generated using the Otsu adaptive thresholding algorithm (Otsu, 1979), which automatically determines the optimal threshold by maximizing inter-class variance. Unlike fixed-threshold approaches, this adaptive method accommodates spatiotemporal variability and has demonstrated robust performance across diverse climatic, hydrological, and land-cover conditions (Chen and Zhao, 2022; Che et al., 2025).

Table 1. Summary of optical satellite datasets used in this study.

Data source	Sensor type	Time coverage	Spatial resolution (m)	Revisit period (days)	Spectral bands
Landsat-5	TM	1990–2011	30	16	Blue, Green, Red, NIR, SWIR1, Thermal IR, SWIR2
Landsat-7	ETM+	1999–2024	15, 30	16	Blue, Green, Red, NIR, SWIR1, SWIR2, Thermal IR, Panchromatic
Landsat-8	OLI	2013–2024	15, 30	16	Coastal aerosol, Blue, Green, Red, NIR, SWIR1, SWIR2, Panchromatic, Cirrus, Thermal IR1, Thermal IR2
Sentinel-2	MSI	2022–2024	10, 20, 60	5 (dual satellite)	Aerosol, Blue, Green, Red, Red Edge 1-4, NIR, Water Vapor, Cirrus, SWIR1, SWIR2

2.2.3 River width estimation and quality control

River width was measured along each predefined cross-section by sampling the binary water mask at the native spatial resolution of each satellite sensor (30 m for Landsat and 10 m for Sentinel-2). The instantaneous river width, W_t, was calculated as:

$$W_t = L \times \frac{N_w}{N_{all}} \quad (2)$$

https://doi.org/10.5194/essd-2026-426
Preprint. Discussion started: 19 June 2026

Open Access Earth System Science Data Discussions

where L is the total cross-section length, defined as $3\bar{W}$; N_w is the number of sampling pixels belonging to the largest connected water body along the cross-section; and N_{all} is the total number of valid sampling points along the cross-section. To ensure the reliability of river width retrievals, width estimates were retained only when N_{all} exceeded 80% of the theoretical maximum number of sampling points (N_{max}). N_{max} is given by:

$$N_{max} = \frac{L}{R} \tag{3}$$

where R denotes the spatial resolution of the satellite sensor (m). This quality-control criterion effectively eliminates low-quality observations affected by cloud contamination, data gaps, or geometric distortions. Additionally, river width estimates smaller than the sensor spatial resolution were discarded as noise.

2.3 River discharge reconstruction and validation

The at-a-station hydraulic geometry (AHG), first introduced by Leopold and Maddock (1953), describes the power-law relationship between river width and discharge at a specific cross-section:

$$W = aQ^b \tag{4}$$

where a and b are empirically derived coefficients representing the scaling relationship between river width and discharge. This relationship has been widely applied to characterize the nonlinear response of river width to discharge variations and has demonstrated strong applicability for satellite-based discharge estimation (Gleason and Wang, 2015; Riggs et al., 2023). Accordingly, the instantaneous river widths derived from satellite imagery (Section 2.2) were paired with concurrent in situ daily discharge observations at each gauge (Section 2.1). To ensure statistical robustness, only gauges with at least ten valid width–discharge pairs (N≥10) were retained for subsequent analysis.

Additional screening procedures were applied to remove gauges exhibiting weak or physically unrealistic width–discharge relationships. First, the Spearman rank correlation coefficient (ρ) was calculated to assess the monotonic association between river width and discharge. Compared with linear correlation metrics, Spearman correlation is less sensitive to outliers and nonlinear behavior and is therefore more suitable for hydraulic geometry analysis (Patidar et al., 2025). Gauges with $\rho < 0.25$ were discarded. Such weak or negative correlations generally indicate that river width does not reliably respond to discharge variability, often due to strong channel confinement, backwater effects, reservoir regulation, or other anthropogenic

https://doi.org/10.5194/essd-2026-426
Preprint. Discussion started: 19 June 2026

disturbances (Eggleston et al., 2024; Wang and Smith, 2025). Second, the fitted hydraulic geometry exponent *b* was evaluated for physical plausibility. In natural river systems, *b* typically ranges between 0 and 0.59, reflecting realistic channel width adjustments under varying flow conditions (Park, 1977; Yuan et al., 2024). Gauges with fitted exponents outside this range were removed to avoid incorporating unstable or physically implausible hydraulic relationships into the discharge reconstruction framework.

To quantitatively evaluate the performance of the satellite-based discharge reconstruction, four commonly used metrics were employed: the Pearson correlation coefficient (CC), normalized root mean square error (NRMSE), relative bias (rBias), and Kling–Gupta efficiency (KGE). These metrics assess different aspects of model performance, including correlation, error magnitude, systematic bias, and overall hydrological consistency. Their formulations are defined as follows:

$$\mathrm{CC} = \frac{\Sigma_{i=1}^{N}\left(\mathrm{Q}_i^{\mathrm{obs}} - \overline{\mathrm{Q}^{\mathrm{obs}}}\right)\left(\mathrm{Q}_i^{\mathrm{est}} - \overline{\mathrm{Q}^{\mathrm{est}}}\right)}{\sqrt{\Sigma_{i=1}^{N}\left(\mathrm{Q}_i^{\mathrm{obs}} - \overline{\mathrm{Q}^{\mathrm{obs}}}\right)^2}\sqrt{\Sigma_{i=1}^{N}\left(\mathrm{Q}_i^{\mathrm{est}} - \overline{\mathrm{Q}^{\mathrm{est}}}\right)^2}} \tag{5}$$

$$\mathrm{N}RMSE = \frac{\sqrt{\frac{1}{N}\Sigma_{i=1}^{N}\left(\mathrm{Q}_i^{\mathrm{est}} - Q_i^{obs}\right)^2}}{\mathrm{Q}_{\mathrm{max}}^{\mathrm{obs}} - \mathrm{Q}_{\mathrm{min}}^{\mathrm{obs}}} \tag{6}$$

$$\mathrm{rB}ias = \frac{\Sigma_{i=1}^{N}\left(\mathrm{Q}_i^{\mathrm{est}} - \mathrm{Q}_i^{\mathrm{obs}}\right)}{\Sigma_{i=1}^{N}\mathrm{Q}_i^{\mathrm{obs}}} \tag{7}$$

where $\mathrm{Q}_i^{\mathrm{obs}}$ and $\mathrm{Q}_i^{\mathrm{est}}$ denote the observed and estimated discharge (m³/s) at time step *i*, respectively. $\overline{\mathrm{Q}^{\mathrm{obs}}}$ and $\overline{\mathrm{Q}^{\mathrm{est}}}$ represent the corresponding mean discharge values, and N is the total number of paired observations.

$$\mathrm{KGE} = 1 - \sqrt{(r-1)^2 + (\alpha-1)^2 + (\beta-1)^2} \tag{8}$$

$$r = \mathrm{CC},\ \alpha = \sigma^{\mathrm{est}}/\sigma^{\mathrm{obs}},\ \beta = \mu^{\mathrm{est}}/\mu^{\mathrm{obs}} \tag{9}$$

where σ^{obs} and σ^{est} represent the standard deviations of the observed and estimated discharge, respectively, while μ^{obs} and μ^{est} denote their mean values.

Compared with traditional performance metrics such as the Nash–Sutcliffe efficiency (NSE), KGE explicitly decomposes model performance into correlation, variability, and bias components, thereby providing a more balanced and diagnostically informative evaluation of hydrological simulations. Owing to these advantages, KGE has been widely adopted in recent studies of remotely sensed discharge estimation, facilitating direct comparison with existing datasets and methodologies (Lin et al., 2023; Riggs et al., 2023; Elmi et al., 2024; Saemian et al., 2024).

https://doi.org/10.5194/essd-2026-426
Preprint. Discussion started: 19 June 2026

Open Access Earth System Science Data Discussions

3 Results

3.1 Evaluation of width–discharge relationships

Following the screening criteria, a total of 310 gauges with sufficient width–discharge observations and physically consistent hydraulic geometry relationships were retained for discharge reconstruction (Fig. 5). The ρ between river width and discharge ranges from 0.26 to 0.99, with a median value of 0.88 and a mean of 0.84 (Fig. 5a, c). The interquartile range (IQR) spans 0.78–0.92, and approximately 70% of the gauges exhibit strong correlations ($\rho > 0.8$), whereas only 1.3% show correlations below 0.5. Additionally, nearly 90% of gauges fall within the range of 0.59–0.96. Spatially, strong width–discharge correlations are widely distributed across diverse hydroclimatic regions of China, whereas weak correlations show no clear geographic clustering (Fig. 5a). These results indicate that river width at the selected gauges responds sensitively and consistently to discharge variability, thereby satisfying a key prerequisite for satellite-based discharge estimation.

The hydraulic geometry exponent b derived from the AHG relationship further supports the physical realism of the width–discharge relationship (Fig. 5b, d). The fitted b values range from 0.039 to 0.530, with a median of 0.217, a mean of 0.243, and an IQR of 0.177–0.303. Approximately 92% of gauges exhibit b values between 0 and 0.4, consistent with previous large-sample hydraulic geometry studies. For example, Park (1977) reported a median b value of ~0.23 based on 139 gauges, while Yuan et al. (2024) found a median value of 0.213 using 436 global gauges, with 94% of gauges falling within the 0–0.4 interval. Notably, relatively high b values (e.g., 0.44 and 0.53) are primarily associated with gauges located in multi-threaded or laterally unconfined river systems (Fig. 5e, f). In these environments, increasing discharge often induces substantial lateral inundation across multiple channels, bars, and floodplain surfaces, thereby enhancing the sensitivity of river width to discharge fluctuations. Such amplified width responses are characteristics of braided and morphodynamically active river systems (Ashmore and Sauks, 2006; Yuan et al., 2024). Overall, these results demonstrate that satellite-derived river widths effectively capture real discharge dynamics and provide a physically robust basis for extending daily river discharge records across the selected gauges.

https://doi.org/10.5194/essd-2026-426
Preprint. Discussion started: 19 June 2026

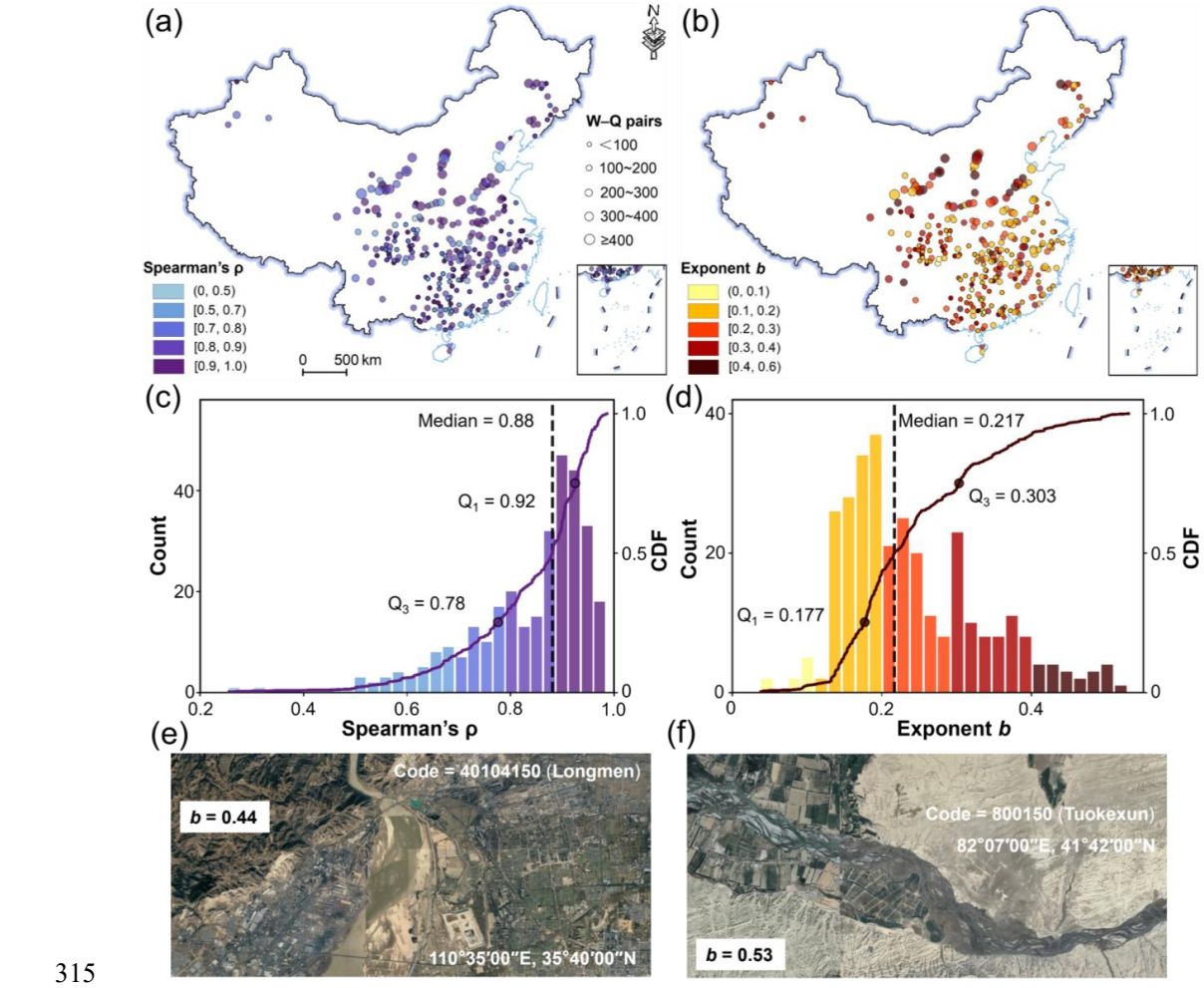

Figure 5. Spatial distribution and statistical characteristics of width–discharge relationships across the 310 selected gauges. (**a**) Spatial distribution of the Spearman rank correlation coefficient (ρ) between river width and discharge, with symbol size representing the number of width–discharge (W–Q) observation pairs at each gauge. (**b**) Spatial distribution of the power-law exponent (b) derived from the at-a-station hydraulic geometry (AHG) relationship. (**c–d**) Frequency histograms and cumulative distribution functions (CDFs) of ρ and b, respectively, with median values and interquartile ranges indicated. (**e–f**) High-resolution satellite imagery of representative river reaches exhibiting high b values and morphologically dynamic channel patterns. Source of the underlying image: © Google Earth.

https://doi.org/10.5194/essd-2026-426
Preprint. Discussion started: 19 June 2026

3.2 Performance evaluation of satellite-extended river discharge

Building upon the robust width–discharge power-law relationships established at 310 gauges, we reconstructed and extended daily river discharge records for the period 1990–2024 and evaluated performance using four complementary metrics. Overall, the satellite-extended discharge exhibits strong agreement with in situ observations (Fig. 6). The median values of the CC, NRMSE, rBias, and KGE are 0.80, 12.67%, 6.56%, and 0.66, respectively. Approximately 73% of gauges exhibit strong correlation (CC > 0.7), while 79% achieve NRMSE values below 20%, indicating that the reconstructed discharge reliably captures both the temporal variability and magnitude of observations across diverse hydrological regimes. Notably, KGE values exceed −0.41 at 96% of gauges, suggesting that the reconstructed discharge consistently outperforms a simple mean discharge benchmark and retains meaningful predictive skill (Knoben et al., 2019). Moreover, 91% of gauges show positive KGE values, demonstrating that the reconstructed records generally reproduce observed discharge dynamics with acceptable overall fidelity. Spatially, gauges with high predictive performance are broadly distributed across China's major river basins, with no obvious concentration in any specific hydroclimatic region. This widespread performance underscores the robustness and scalability of the proposed framework and demonstrates the strong potential of integrating satellite-derived river width with AHG relationships to reconstruct daily river discharge over large spatial domains.

https://doi.org/10.5194/essd-2026-426
Preprint. Discussion started: 19 June 2026

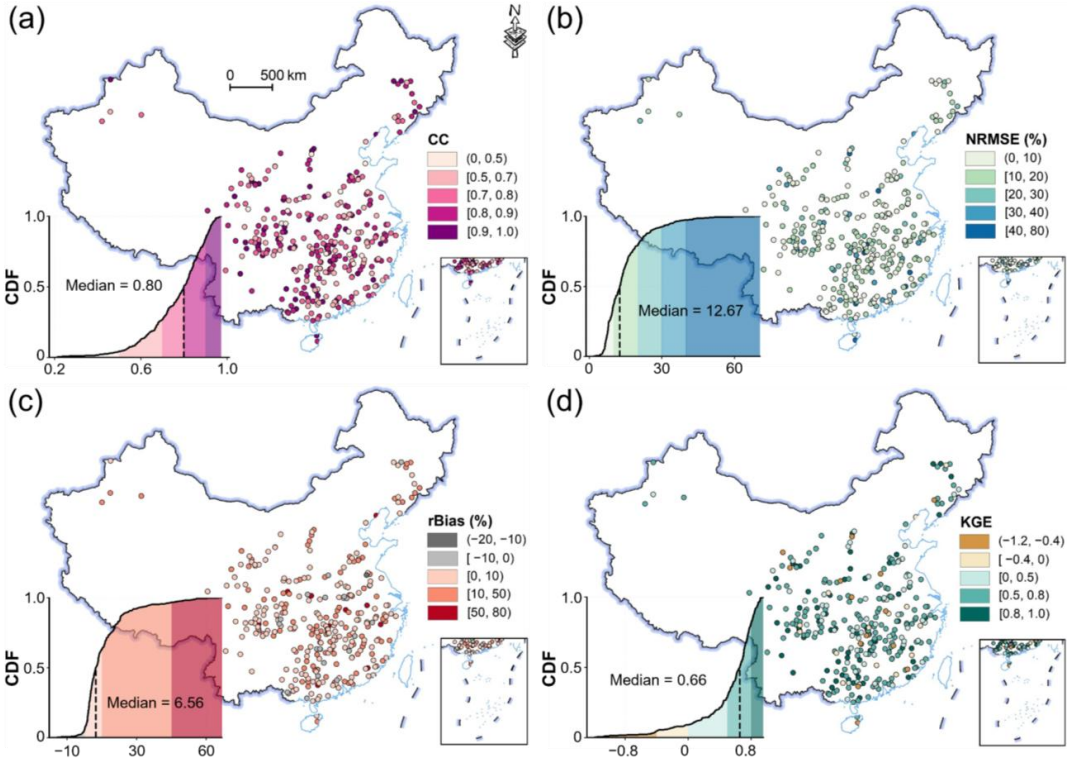

Figure 6. Performance evaluation of satellite-extended river discharge across 310 gauges based on the AHG width–discharge power-law relationship. (**a–d**) Spatial distributions of the Pearson correlation coefficient (CC), normalized root mean square error (NRMSE, %), relative bias (rBias, %), and Kling–Gupta efficiency (KGE), respectively. Insets in each panel present the corresponding cumulative distribution functions (CDFs), with median values indicated.

To further investigate how reconstruction performance depends on river dynamism, the selected gauges were stratified into five equal-frequency groups (G1–G5) according to the coefficient of variation of river width (CV_w), with group mean values ranging from 6% to 23% (Fig. 7). Performance metrics were then compared across the CV_w gradient. The results reveal a clear positive relationship between discharge reconstruction performance and river width variability. Specifically, both NRMSE and rBias decrease with increasing CV_w (Fig. 7b, c), while KGE increases correspondingly (Fig. 7d), with all trends statistically significant ($p < 0.05$). These findings are physically consistent with expectations, as rivers exhibiting greater morphological variability generally respond more sensitively to discharge fluctuations. Such enhanced hydraulic responsiveness improves the detectability of width changes in satellite observations and

https://doi.org/10.5194/essd-2026-426
Preprint. Discussion started: 19 June 2026

strengthens the robustness of width-based discharge estimation (Durand et al., 2023; Lin et al., 2023; Scherer et al., 2024). Although CC does not exhibit a statistically significant monotonic trend (p = 0.11), the relatively high coefficient of determination (R^2 = 0.62) still suggests a moderate positive association with CV_w (Fig. 7a). However, CC values remain consistently high (>0.75) across all groups, with only limited intergroup variability, indicating that the temporal dynamics of river discharge are effectively captured regardless of river width variability. Notably, even within the low-CV_w groups, where predictive performance is comparatively weaker, the reconstruction framework retains satisfactory skill, with median CC, NRMSE, rBias, and KGE values of approximately 0.76, 15.97%, 9.65%, and 0.55, respectively. These results demonstrate that reliable discharge reconstruction can still be achieved in rivers with relatively limited width variability, highlighting the robustness and broad applicability of the proposed framework across diverse channel morphologies and hydrological conditions.

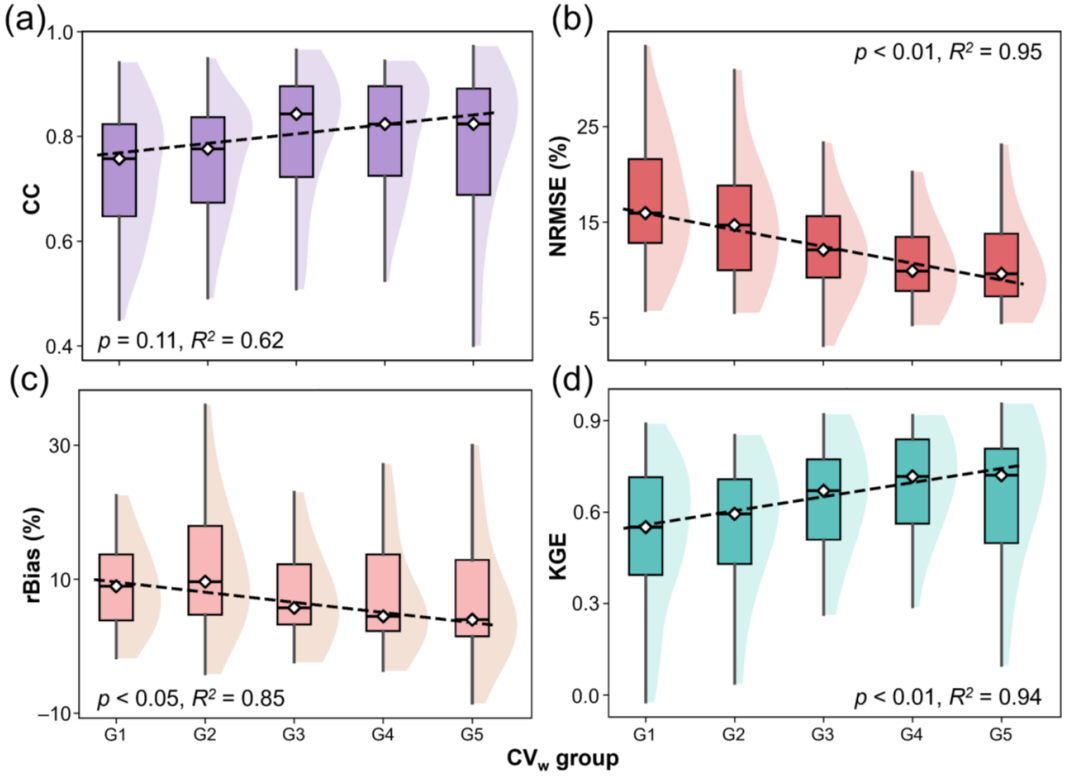

Figure 7. Performance evaluation of satellite-extended discharge across gradients of river width variability, quantified by the coefficient of variation of river width (CV_w). (**a–d**) Boxplots of performance metrics, including the Pearson correlation coefficient (CC), normalized root mean

https://doi.org/10.5194/essd-2026-426
Preprint. Discussion started: 19 June 2026

square error (NRMSE), relative bias (rBias), and Kling–Gupta efficiency (KGE), for the 310 gauges grouped into five equal-frequency classes according to CV_w. Outliers are not shown for clarity. Dashed lines indicate linear regression fits to the group median values, with corresponding significance levels (p) and coefficients of determination (R^2) shown in each panel.

3.3 Long-term trends and observation frequency of satellite-extended river discharge

Using the satellite-extended daily discharge records from 310 gauges spanning 1990–2024, we quantified the long-term trends and observational characteristics of rivers across China (Fig. 8). Trend detection was performed using the non-parametric Mann-Kendall test (Mann, 1945) in combination with Sen's slope estimator (Sen, 1968), applied to annually aggregated discharge series. Relative annual rates of change (%/yr) were calculated by normalizing Sen's slope with the multi-year mean discharge, thereby facilitating comparison among rivers with varying discharge magnitudes. To improve the robustness of trend estimation, only years containing at least three observations separated by a minimum intra-annual interval of six months were retained. Furthermore, trend analysis was restricted to gauges with more than 15 valid years of records. After quality filtering, 309 gauges were included in the final analysis, with an average effective record length of 32.5 years.

The results reveal a subtle but widespread decline in river discharge across China, with approximately 65% (n = 201) of gauges exhibiting negative trends and a median relative change rate of −0.21%/yr (Fig. 8a). Spatially, declining trends are concentrated in northern and central China, particularly within the Haihe, Liaohe, and Yellow River basins, as well as parts of the middle Yangtze River basin. This pattern is consistent with recent assessments suggesting that discharge reductions in these regions are primarily driven by geomorphological alterations, further intensified by anthropogenic water management activities such as water abstraction, inter-basin diversion, and reservoir regulation (Yang et al., 2022; Wang et al., 2025a). In terms of trend magnitude, most declining gauges (n = 180) exhibit relatively modest decreases of less than 2%/yr, whereas 21 gauges show declines exceeding this threshold. Importantly, a persistent decrease greater than 2%/yr corresponds to a cumulative reduction exceeding 40% over the past three decades, indicating substantial long-term discharge loss at these locations. Statistical significance testing identifies monotonic trends at 141 gauges (46% of all analyzed gauges, $p < 0.1$), among which 61% exhibit declining discharge. Within the significantly declining subset, 66 gauges

https://doi.org/10.5194/essd-2026-426
Preprint. Discussion started: 19 June 2026

decrease by less than 2%/yr, while 20 gauges decline by more than 2%/yr. Conversely, 108 gauges exhibit increasing discharge trends, of which approximately 51% are statistically significant. These increasing trends are primarily concentrated in the northwestern and middle-to-lower Yangtze River basin, the northern Pearl River basin, and the upper Yellow River basin. Overall, the spatial heterogeneity of discharge trends reflects the diverse and complex hydrological responses occurring across China's distinct geographical and hydroclimatic regions.

The temporal sampling characteristics of the satellite-extended discharge dataset were further examined (Fig. 8b). The median number of observations per gauge is 375, corresponding to approximately 11 observations per year, while about 42% of gauges contain more than 420 observations (≥12 observations per year). Despite this generally dense temporal coverage, observation frequency exhibits substantial spatial heterogeneity across China. Gauges with fewer than 300 observations are predominantly concentrated in the middle Yangtze and Pearl River basins. This reduced sampling density is primarily associated with persistent cloud cover, frequent precipitation, and complex topography, which limit the availability of high-quality optical satellite imagery and consequently reduce the number of usable observations. Nevertheless, even under irregular observational intervals, the reconstructed discharge records preserve key hydrological dynamics. For example, the reconstructed time series at the Dalai (Fig. 8c) and Longmenzhen (Fig. 8d) gauges successfully capture transitions from baseflow to peak-flow conditions while maintaining coherent multidecadal variability and long-term discharge trends. These examples demonstrate that the satellite-based reconstruction framework can resolve both short-term hydrological fluctuations and long-term discharge despite the discontinuous sampling inherent in optical remote sensing observations. Overall, these results indicate that the satellite-extended discharge dataset provides sufficient temporal depth and observational frequency to support robust gauge-scale trend analysis, offering valuable insights into the long-term hydrological evolution of China's major river systems.

https://doi.org/10.5194/essd-2026-426
Preprint. Discussion started: 19 June 2026

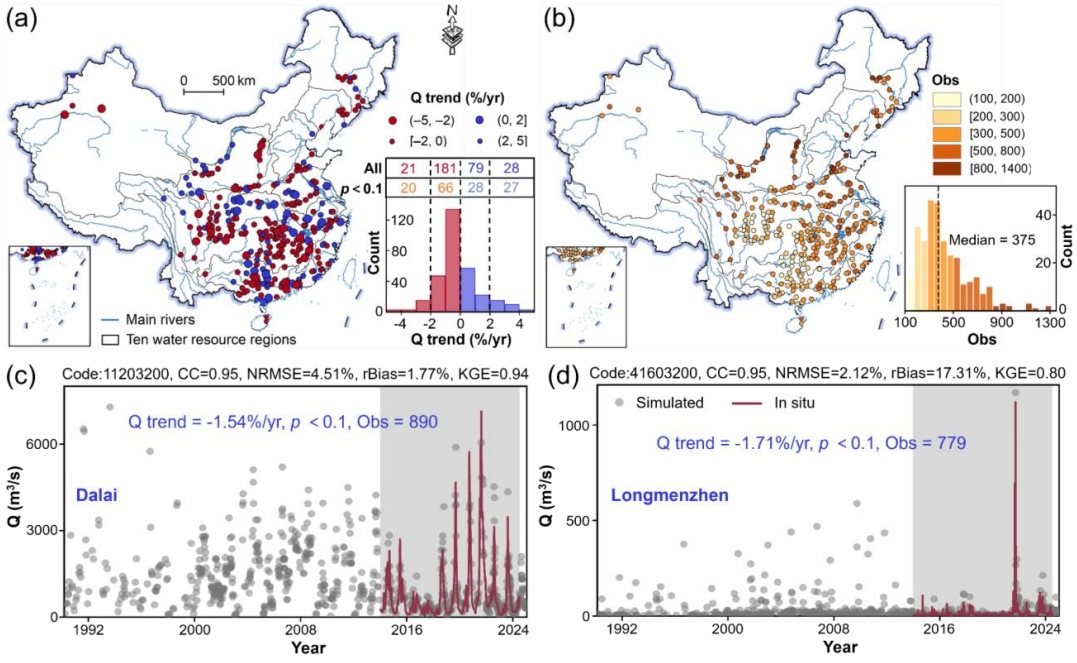

Figure 8. Spatial patterns and long-term trends of satellite-extended river discharge across 309 gauges in China (1990–2024). (**a**) Spatial distribution of relative discharge change rates (Q trend, %/yr), normalized by multi-year mean discharge, with inset histograms showing the trend distribution and corresponding significance levels (*p*) across all gauges. (**b**) Spatial distribution of additional observation (Obs) provided by the satellite-extended discharge records at each gauge. (**c–d**) Representative time series of reconstructed daily discharge at Dalai and Longmenzhen gauges, respectively, illustrating long-term discharge variability and trends together with corresponding model performance metrics.

4 Discussion

4.1 Comparison of reconstructed discharge records with existing datasets

To better contextualize the contribution of the CDR^2 dataset, we conducted a comparative assessment against several representative global remotely sensed river discharge products, including the Remote Sensing-based Extension for the GRDC (RSEG) (Elmi et al., 2024), the Satellite Altimetry-based Extension of global in situ river discharge Measurements (SAEM) (Saemian et al., 2024), and the datasets developed by Lin et al. (2023) and Riggs et al. (2023). Although these datasets have substantially expanded the spatial coverage of global river discharge

https://doi.org/10.5194/essd-2026-426
Preprint. Discussion started: 19 June 2026


Open Access Earth System Science Data Discussions

observations, their representation within China remains extremely limited (Fig. 9 and Table 2). Specifically, the number of gauges in China ranges from only one in Riggs et al. (2023) to 62 in SAEM. In all cases, Chinese gauges account for less than 1% of the total stations included in these global products, reflecting both the scarcity of publicly accessible in situ discharge observations and the challenges of satellite-based discharge retrieval in this region. In contrast, CDR^2 increases the number of gauge-constrained discharge records within China by approximately 5–300 times relative to existing global datasets, providing daily discharge reconstructions at 310 gauges distributed across diverse hydroclimatic and geomorphological settings (Fig. 9). The dataset encompasses rivers spanning a wide range of discharge magnitudes and channel sizes, thereby substantially improving the representation of China within global river discharge archives.

Beyond its improved spatial coverage, CDR^2 also demonstrates clear advantages in temporal resolution and predictive performance. While RSEG and Lin et al. (2023) provide monthly discharge estimates, CDR^2, SAEM, and Riggs et al. (2023) operate at daily time scales. Notably, CDR^2 achieves a median KGE of 0.66, substantially outperforming the reported global median range of 0.33–0.48 among existing products (Table 2). Consistent improvements are also evident in other performance metrics, including a lower median NRMSE (12.7%) and a higher median CC (0.80), indicating enhanced capability in reproducing both the magnitude and temporal variability of observed discharge.

These improvements are partly attributed to the rigorous screening strategy adopted in this study, whereby only gauges exhibiting stable width–discharge relationships and physically consistent hydraulic behavior were retained (Fig. 5). In contrast, global-scale products often face an inherent trade-off between maximizing spatial coverage and maintaining retrieval quality, frequently incorporating gauges with weaker hydraulic relationships or unstable channel responses that introduce additional uncertainty. Moreover, by integrating observations from both Landsat and Sentinel-2 imagery, CDR^2 achieves a substantially higher effective sampling frequency than single-sensor approaches. This enhanced temporal sampling improves detection of short-term discharge fluctuations and mitigates the smoothing effects of monthly aggregation, as observed in RSEG and Lin et al. (2023), thereby enabling a more realistic reconstruction of daily discharge dynamics. Overall, CDR^2 provides a substantially improved and higher-resolution characterization of river discharge across China, a hydrologically critical yet globally underrepresented region.

https://doi.org/10.5194/essd-2026-426
Preprint. Discussion started: 19 June 2026

Through its greatly expanded gauge density, daily temporal resolution, and enhanced predictive performance, the dataset fills a major geographic gap in existing global river discharge products.

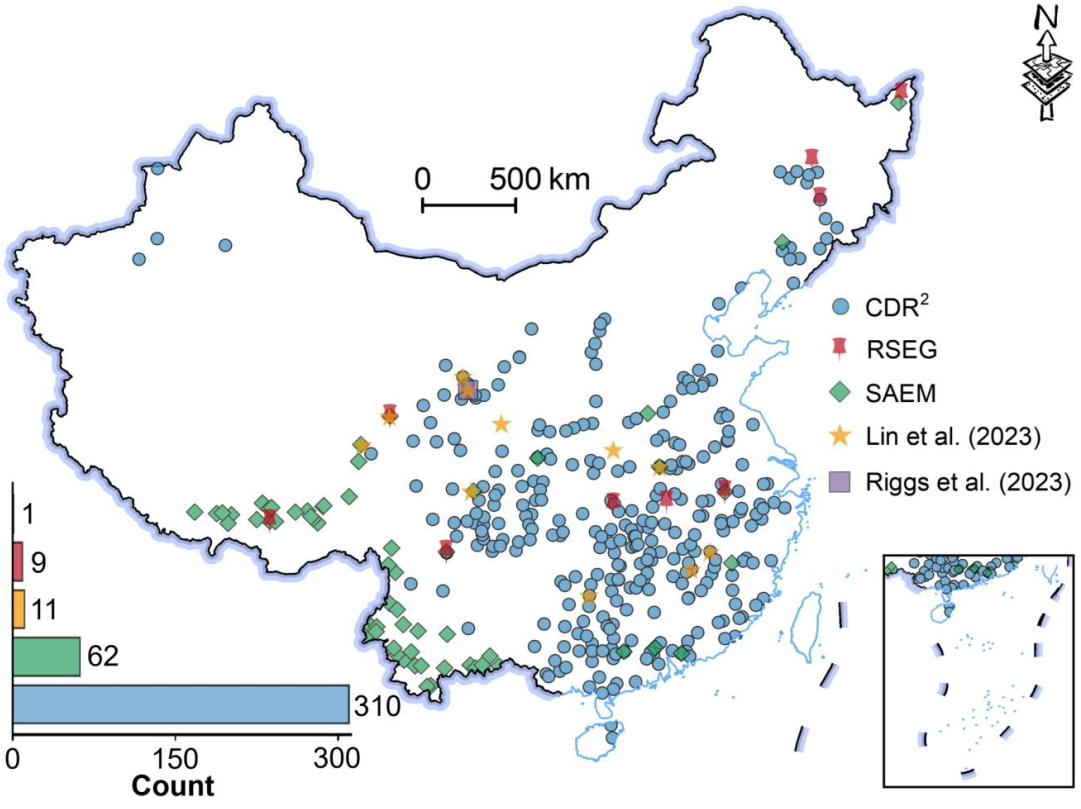

Figure 9. Spatial distribution of river discharge gauges included in CDR^2, compared with gauges from RSEG (Elmi et al., 2024), SAEM (Saemian et al., 2024), Lin et al. (2023), and Riggs et al. (2023). The inset summarizes the number of gauges contained in each dataset within China.

Table 2. Comparison of CDR^2 with existing satellite-extended river discharge datasets.

Dataset	Hydraulic variables	Data source	Global gauge	China gauge	Temporal resolution	Validation results
Elmi et al., 2024 (RSEG)	River width/ stage	Landsat/Satellite altimetry	3377	9	Monthly	All gauges (mean): KGE = 0.35, rRMSE = 21.8%, CC = 0.43
Saemian et al., 2024 (SAEM)	River stage	Satellite altimetry	8730	62	Daily	All gauges (median): KGE = 0.48, nRMSE = 18%, CC = 0.64
Lin et al., 2023	River width	Landsat	3078	11	Monthly	>600 gauges (median): KGE = 0.33
Riggs et al., 2023	River width	Landsat/Sentinel	2168	1	Daily	All gauges (median): KGE = 0.46, rRMSE = 83%, rBias = 1.4%
CDR^2	River width	Landsat/Sentinel	310	310	Daily	All gauges (median): KGE = 0.66, nRMSE = 12.7%, rBias = 6.6%, CC = 0.8

https://doi.org/10.5194/essd-2026-426
Preprint. Discussion started: 19 June 2026

4.2 Sensitivity of reconstruction performance to the width–discharge exponent

To investigate how hydraulic controls influence discharge reconstruction accuracy, we evaluated the sensitivity of model performance to the width–discharge exponent b (Fig. 10). This exponent characterizes the responsiveness of river width to discharge variability and therefore serves as a key hydraulic link between satellite-observed channel dynamics and river discharge behavior. The analysis reveals statistically significant relationships between b and multiple performance metrics (Fig. 10a–c). Specifically, both NRMSE and rBias exhibit significant negative correlations with b ($\rho = -0.46$ and -0.49, respectively; $p < 0.001$), whereas KGE shows a significantly positive correlation ($\rho = 0.52$, $p < 0.001$). These results indicate that rivers with greater hydraulic sensitivity experience larger width variations under comparable discharge fluctuations, making these changes more readily detectable by satellite observations (Fig. 7) and thereby mitigating the propagation of observational uncertainty into discharge reconstruction.

To identify a robust threshold for hydraulic sensitivity, gauges were first sorted according to increasing b values, after which a sliding-window analysis was applied to evaluate local gradients of each performance metric with respect to b. To facilitate comparison across metrics with different numerical ranges, the gradients were normalized to their respective global ranges. The optimal threshold (b_{opt}) was defined as the point at which the absolute normalized gradient consistently declined below 20% of its global maximum, indicating that performance stabilizes beyond this value. The intersection of these stabilization regions across all metrics yields a global threshold of $b = 0.25$ (Fig. 10d). Below this threshold, large fluctuations in normalized gradients indicate considerable uncertainty in discharge reconstruction for hydraulically constrained rivers. Once b exceeds 0.25, all gradients converge toward zero, suggesting that width-based discharge estimation becomes substantially more stable and reliable for rivers with stronger hydraulic responsiveness.

The contrasting influence of b on reconstruction performance is clearly illustrated by the Zhangjiajie and Wutongqiao (II) gauges (Fig. 10e, f). At Zhangjiajie, characterized by a low b value, substantial discharge variability corresponds to only marginal changes in river width, often approaching the spatial resolution limit of the satellite sensor (~30 m). Under such conditions, the inversion from width to discharge becomes mathematically ill-conditioned, whereby small uncertainties in width retrieval propagate into disproportionately large discharge errors, ultimately degrading reconstruction performance (Fig. 10e). In contrast, the Wutongqiao (II) gauge exhibits a high b value, where pronounced width sensitivity to discharge allows satellite observations to

https://doi.org/10.5194/essd-2026-426
Preprint. Discussion started: 19 June 2026

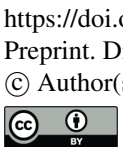

Open Access Earth System Science Data Discussions

effectively resolve discharge variations across the full hydrological spectrum, from low-flow conditions to flood peaks. Together, these findings demonstrate that *b* provides a physically meaningful and robust criterion for identifying rivers suitable for reliable satellite-based discharge reconstruction, offering important guidance for future large-scale discharge estimation and monitoring efforts.

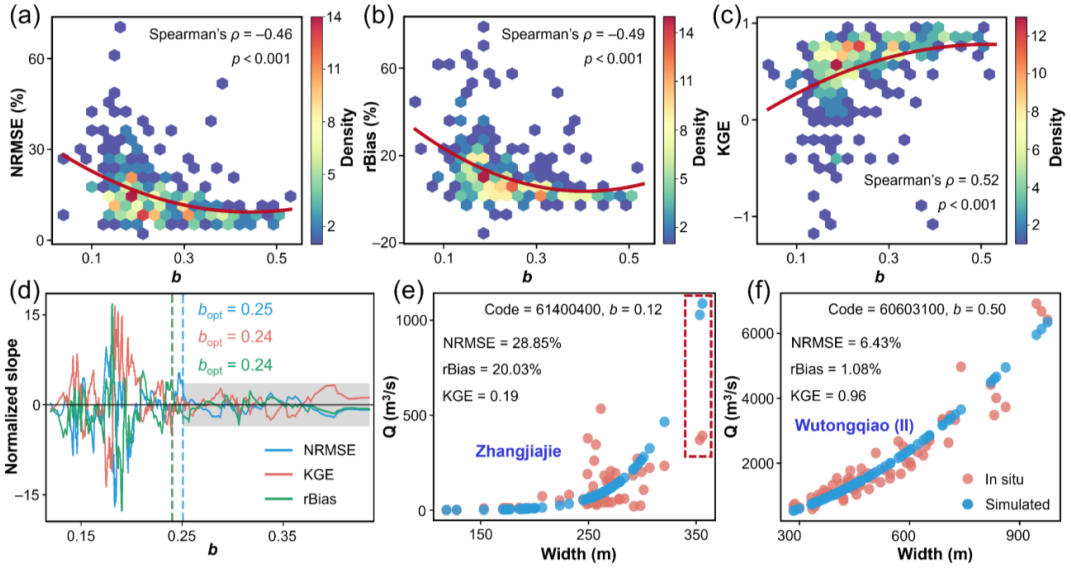

Figure 10. Influence of the width–discharge power-law exponent (*b*) on the performance of satellite-extended discharge reconstruction. (**a–c**) Relationships between the hydraulic geometry exponent (*b*) and the performance metrics NRMSE, rBias, and KGE, respectively. Red solid lines indicate fitted relationships, with the corresponding Spearman rank correlation coefficient (ρ) and significance level (p) indicated. (**d**) Variation in the normalized slope of performance metrics with respect to *b*, used to identify the optimal threshold (b_{opt}) beyond which reconstruction performance becomes stable and less sensitive to changes in hydraulic responsiveness. (**e–f**) Comparison between in situ and reconstructed discharge at the Zhangjiajie and Wutongqiao (II) gauges, representing examples of low-*b* and high-*b* hydraulic conditions, respectively.

5 Data availability

The China Daily River Discharge Records (CDR^2) dataset developed in this study is publicly available on Zenodo at https://doi.org/10.5281/zenodo.20152832 (Wang and Li, 2026). The dataset is distributed in CSV format, with each file named according to its corresponding gauge

https://doi.org/10.5194/essd-2026-426
Preprint. Discussion started: 19 June 2026

ID. It contains reconstructed daily river discharge records for 310 gauges across China, along with the associated width–discharge power-law relationships, covering the period from 1990 to 2024.

The in situ daily river discharge observations were sourced from the National Hydrological and Rainfall Information System of the Ministry of Water Resources of China (http://xxfb.mwr.cn/). The Global Runoff Data Centre (GRDC) data can be accessed at:https://portal.grdc.bafg.de/applications/public.html?publicuser=PublicUser. The Chinese Hydrology Project (CHP) data are not publicly available and were provided by the dataset's authors (Henck et al., 2010; Schmidt et al., 2011). The Surface Water and Ocean Topography River Database (Version v17) is available at: https://zenodo.org/records/14727521. All Landsat-5/7/8 and Sentinel-2 optical remote sensing data were accessed via the Google Earth Engine platform (https://earthengine.google.com/). The following publicly available global satellite-based river discharge products were used for comparison. Satellite Altimetry-based Extension of global in situ river discharge Measurements (SAEM) is available at: https://doi.org/10.18419/darus-4475. Remote Sensing-based Extension for the GRDC (RSEG) is available at: https://doi.org/10.18419/darus-3558. Datasets developed by Lin et al. (2023) and Riggs et al. (2023), which can be accessed at: https://zenodo.org/records/6655532#.Yqw37XZBz-g and https://zenodo.org/record/7150168#.ZAow8RXMIuV.

6 Conclusions

This study integrates multi-decadal optical remote sensing observations, a robust at-a-station hydraulic geometry (AHG) width–discharge framework, and in situ daily discharge records from 1,196 gauging stations to develop the China Daily River Discharge Records (CDR^2), a high-resolution satellite-extended daily discharge dataset spanning 1990–2024 for 310 gauges across China. Validation against in situ observations demonstrates that CDR^2 accurately captures both the temporal dynamics and magnitude of river discharge, achieving median values of 0.66 for Kling–Gupta Efficiency (KGE), 0.80 for the Pearson correlation coefficient (CC), 6.56% for relative bias (rBias), and 12.7% for normalized root mean square error (NRMSE). Notably, 91% of gauges exhibit positive KGE values, approximately 73% achieve CC values greater than 0.7, and 79% maintain NRMSE below 20%.

Compared with existing global satellite-based discharge datasets, CDR^2 expands the spatial coverage of daily river discharge monitoring across China by more than fivefold and demonstrates

https://doi.org/10.5194/essd-2026-426
Preprint. Discussion started: 19 June 2026

substantially improved accuracy. Sensitivity analyses further reveal a strong positive relationship between reconstruction performance and river width variability, indicating that satellite observations more effectively resolve rivers exhibiting greater hydraulic responsiveness to discharge fluctuations. Long-term trend analysis reveals a widespread decline in river discharge across China over the past 35 years, with approximately 65% of gauges exhibiting decreasing trends. The median relative rate of change is −0.21%/yr, corresponding to an estimated cumulative reduction of ~7% relative to the long-term mean discharge. These decreases are particularly pronounced in northern and central basins, highlighting increasing spatial disparities in regional hydrological dynamics and underscoring the need for sustained, high-quality discharge monitoring. By substantially expanding gauge-scale discharge observations across China, CDR^2 provides a critical empirical foundation for calibrating next-generation satellite missions and advancing large-scale river discharge estimates in the era of the Surface Water and Ocean Topography (SWOT).

Author contributions

YW performed the investigation, methodology, formal analysis, software, data curation, visualization, and validation, and wrote the original draft. YG curated the data and reviewed and edited the manuscript. YJ performed formal analysis and reviewed and edited the manuscript. XS reviewed and edited the manuscript. YL conceptualized the study, developed the methodology, conducted formal analysis, provided resources, supervised the research, administered the project, acquired funding, and reviewed and edited the manuscript.

Declaration of Competing Interest

The authors declare that they have no known competing financial interests or personal relationships that could have appeared to influence the work reported in this paper.

Acknowledgments

The authors gratefully acknowledge the data providers whose contributions were essential to this study.

Financial support

This work was supported by the National Natural Science Foundation of China (42571446 and 42201349), the Chongqing Doctoral Student Research Innovation Project (CYB240107), and the

https://doi.org/10.5194/essd-2026-426
Preprint. Discussion started: 19 June 2026

592 Chongqing Municipal Science and Technology Bureau (CSTB2024YCJH-KYXM0054 and
593 cstc2024ycjh-bgzxm0043).

https://doi.org/10.5194/essd-2026-426
Preprint. Discussion started: 19 June 2026

References

Allen, G. H., Pavelsky, T. M.: Global extent of rivers and streams, Science, 361, 585–588, https://doi.org/10.1126/science.aat0636, 2018.

Alsdorf, D. E., Rodríguez, E., Lettenmaier, D. P.: Measuring surface water from space, Rev. Geophys., 45, RG2002, https://doi.org/10.1029/2006RG000197, 2007.

Altenau, E. H., Pavelsky, T. M., Durand, M. T., Yang, X., Frasson, R. P. M., and Bendezu, L.: The Surface Water and Ocean Topography (SWOT) Mission River Database (SWORD): A global river network for satellite data products, Water Resour. Res., 57, e2021WR030054, https://doi.org/10.1029/2021WR030054, 2021.

Andrews, L. and Grantham, T. E.: Strategic stream gauging network design for sustainable water management, Nat. Sustain., 7, 714–723, https://doi.org/10.1038/s41893-024-01357-z, 2024.

Ashmore, P. and Sauks, E.: Prediction of discharge from water surface width in a braided river with implications for at-a-station hydraulic geometry, Water Resour. Res., 42, W03407, https://doi.org/10.1029/2005WR003993, 2006.

Beven, K.: Towards integrated environmental models of everywhere: uncertainty, data and modelling as a learning process, Hydrol. Earth Syst. Sci., 11, 460–467, https://doi.org/10.5194/hess-11-460-2007, 2007.

Bonnema, M. G., Sikder, S., Hossain, F., Durand, M., Gleason, C. J., and Bjerklie, D. M.: Benchmarking wide swath altimetry-based river discharge estimation algorithms for the Ganges river system, Water Resour. Res., 52, 2439–2461, https://doi.org/10.1002/2015WR017296, 2016.

Che, L., Li, S., and Liu, X.: Improved surface water mapping using satellite remote sensing imagery based on optimization of the Otsu threshold and effective selection of remote-sensing water index, J. Hydrol., 654, 132771, https://doi.org/10.1016/j.jhydrol.2025.132771, 2025.

Chen, Z. and Zhao, S.: Automatic monitoring of surface water dynamics using Sentinel-1 and Sentinel-2 data with Google Earth Engine, Int. J. Appl. Earth Obs. Geoinf., 113, 103010, https://doi.org/10.1016/j.jag.2022.103010, 2022.

Collins, E. L., David, C. H., Riggs, R., Allen, G. H., Pavelsky, T. M., Lin, P., Pan, M., Yamazaki, D., Meentemeyer, R. K., and Sanchez, G. M.: Global patterns in river water storage dependent on residence time, Nat. Geosci., 17, 433–439, https://doi.org/10.1038/s41561-024-01421-5, 2024.

https://doi.org/10.5194/essd-2026-426
Preprint. Discussion started: 19 June 2026

625 Do, H. X., Gudmundsson, L., Leonard, M., and Westra, S.: The Global Streamflow Indices and
626 Metadata Archive (GSIM)–Part 1: The production of a daily streamflow archive and metadata,
627 Earth Syst. Sci. Data, 10, 765–785, https://doi.org/10.5194/essd-10-765-2018, 2018.
628 Durand, M., Gleason, C. J., Garambois, P. A., Bjerklie, D., Smith, L. C., Roux, H., Rodriguez, E.,
629 Bates, P. D., Pavelsky, T. M., Monnier, J., Chen, X., Di Baldassarre, G., Fiset, J.-M., Flipo,
630 N., Frasson, R. P. d. M., Fulton, J., Goutal, N., Hossain, F., Humphries, E., Minear, J. T.,
631 Mukolwe, M. M., Neal, J. C., Ricci, S., Sanders, B. F., Schumann, G., Schubert, J. E., and
632 Vilmin, L.: An intercomparison of remote sensing river discharge estimation algorithms from
633 measurements of river height, width, and slope, Water Resour. Res., 52, 4527–4549,
634 https://doi.org/10.1002/2015WR018434, 2016.
635 Durand, M., Gleason, C. J., Pavelsky, T. M., Frasson, R. P. M., Turmon, M., David, C. H., Altenau,
636 E. H., Tebaldi, N., Larnier, K., Monnier, J., Malaterre, P. O., Oubanas, H., Allen, G. H.,
637 Astifan, B., Brinkerhoff, C., Bates, P. D., Bjerklie, D., Coss, S., Dudley, R., Fenoglio, L.,
638 Garambois, P.-A., Getirana, A., Lin, P., Margulis, S. A., Matte, P., Minear, J. T., Muhebwa,
639 A., Pan, M., Peters, D., Riggs, R., Sikder, M. S., Simmons, T., Stuurman, C., Taneja, J.,
640 Tarpanelli, A., Schulze, K., Tourian, M. J., and Wang, J.: A framework for estimating global
641 river discharge from the Surface Water and Ocean Topography satellite mission, Water
642 Resour. Res., 59, e2021WR031614, https://doi.org/10.1029/2021WR031614, 2023.
643 Eggleston, J., Mason, C., Bjerklie, D., Durand, M., Dudley, R., and Harlan, M.: Siting
644 considerations for satellite observation of river discharge, Water Resour. Res., 60,
645 e2023WR034583, https://doi.org/10.1029/2023WR034583, 2024.
646 Elmi, O., Tourian, M. J., Saemian, P., and Sneeuw, N.: Remote sensing-based extension of GRDC
647 Discharge time series – a monthly product with uncertainty estimates, Sci. Data, 11, 240,
648 https://doi.org/10.1038/s41597-024-03078-6, 2024.
649 Famiglietti, J. S., Cazenave, A., Eicker, A., Reager, J. T., Rodell, M., and Velicogna, I.: Satellites
650 provide the big picture, Science, 349, 684–685, https://doi.org/10.1126/science.aac9238,
651 2015.
652 Färber, C., Plessow, H., Mischel, S. A., Kratzert, F., Addor, N., Shalev, G., and Looser, U.:
653 GRDC-Caravan: extending caravan with data from the global runoff data centre, Earth Syst.
654 Sci. Data, 17, 4613–4625, https://doi.org/10.5194/essd-17-4613-2025, 2025.

https://doi.org/10.5194/essd-2026-426
Preprint. Discussion started: 19 June 2026

655 Fekete, B. M., Robarts, R. D., Kumagai, M., Nachtnebel, H.-P., Odada, E., and Zhulidov, A. V.:
656 Time for in situ renaissance, Science, 349, 685–686, https://doi.org/10.1126/science.aac7358,
657 2015.
658 Feng, D., Gleason, C. J., Yang, X., and Pavelsky, T. M.: Comparing discharge estimates made via
659 the BAM algorithm in high-order Arctic rivers derived solely from optical CubeSat, Landsat,
660 and Sentinel-2 data, Water Resour. Res., 55, 7753–7771,
661 https://doi.org/10.1029/2019WR025599, 2019.
662 Ghiggi, G., Humphrey, V., Seneviratne, S. I., and Gudmundsson, L.: GRUN: an observation-based
663 global gridded runoff dataset from 1902 to 2014, Earth Syst. Sci. Data, 11, 1655–1674,
664 https://doi.org/10.5194/essd-11-1655-2019, 2019.
665 Gleason, C. J. and Smith, L. C.: Toward global mapping of river discharge using satellite images
666 and at-many-stations hydraulic geometry, Proc. Natl. Acad. Sci. U. S. A., 111, 4788–4791,
667 https://doi.org/10.1073/pnas.1317606111, 2014.
668 Gleason, C. J. and Wang, J.: Theoretical basis for at-many-stations hydraulic geometry, Geophys.
669 Res. Lett., 42, 7107–7114, https://doi.org/10.1002/2015GL064935, 2015.
670 Hannah, D. M., Demuth, S., van Lanen, H. A. J., Looser, U., Prudhomme, C., Rees, G., Stahl, K.,
671 and Tallaksen, L. M.: Large-scale river flow archives: Importance, current status and future
672 needs, Hydrol. Process., 25, 1191–1200, https://doi.org/10.1002/hyp.7794, 2011.
673 Hao, Z., Xiang, N., Cai, X., Zhong, M., Jin, J., Du, Y., and Ling, F.: Remote sensing of river
674 discharge from medium-resolution satellite imagery based on deep learning, Water Resour.
675 Res., 60, e2023WR036880, https://doi.org/10.1029/2023WR036880, 2024.
676 Henck, A. C., Montgomery, D. R., Huntington, K. W., and Liang, C.: Monsoon control of effective
677 discharge, Yunnan and Tibet, Geology, 38, 975–978, https://doi.org/10.1130/G31444.1, 2010.
678 Hou, J., van Dijk, A. I. J. M., and Beck, H. E.: Global satellite-based river gauging and the
679 influence of river morphology on its application, Remote Sens. Environ., 239, 111629,
680 https://doi.org/10.1016/j.rse.2019.111629, 2020.
681 Knoben, W. J. M., Freer, J. E., and Woods, R. A.: Inherent benchmark or not? Comparing Nash–
682 Sutcliffe and Kling–Gupta efficiency scores, Hydrol. Earth Syst. Sci., 23, 4323–4331,
683 https://doi.org/10.5194/hess-23-4323-2019, 2019.
684 Krabbenhoft, C. A., Allen, G. H., Lin, P., Godsey, S. E., Allen, D. C., Burrows, R. M., DelVecchia,
685 A. G., Fritz, K. M., Shanafield, M., Burgin, A. J., Zimmer, M. A., Datry, T., Dodds, W. K.,

https://doi.org/10.5194/essd-2026-426
Preprint. Discussion started: 19 June 2026

686 Jones, C. N., Mims, M. C., Franklin, C., Hammond, J. C., Zipper, S., Ward, A. S., Costigan,
687 K. H., Beck, H. E., and Olden, J. D.: Assessing placement bias of the global river gauge
688 network, Nat. Sustain., 5, 586–592, https://doi.org/10.1038/s41893-022-00873-0, 2022.
689 Leopold, L. B. and Maddock, T.: The hydraulic geometry of stream channels and some
690 physiographic implications, U.S. Government Printing Office, Washington, DC,
691 https://pubs.usgs.gov/pp/0252/report.pdf (last access: 12 March 2026), 1953.
692 Lettenmaier, D. P., Alsdorf, D., Dozier, J., Huffman, G. J., Pan, M., and Wood, E. F.: Inroads of
693 remote sensing into hydrologic science during the WRR era, Water Resour. Res., 51, 7309–
694 7342, https://doi.org/10.1002/2015WR017616, 2015.
695 Lin, P., Pan, M., Beck, H. E., Yang, Y., Yamazaki, D., Frasson, R., David, C. H., Durand, M.,
696 Pavelsky, T. M., Allen, G. H., Gleason, C. J., and Wood, E. F.: Global reconstruction of
697 naturalized river flows at 2.94 million reaches, Water Resour. Res., 55, 6499–6516,
698 https://doi.org/10.1029/2019WR025287, 2019.
699 Lin, P., Feng, D., Gleason, C. J., Pan, M., Brinkerhoff, C. B., Yang, X., Beck, H. E., and Frasson,
700 R. P. d. M.: Inversion of river discharge from remotely sensed river widths: A critical
701 assessment at three-thousand global river gauges, Remote Sens. Environ., 287, 113489,
702 https://doi.org/10.1016/j.rse.2023.113489, 2023.
703 Mann, H. B.: Nonparametric tests against trend, Econometrica, 13, 245–259,
704 https://doi.org/10.2307/1907187, 1945.
705 McFeeters, S. K.: The use of the Normalized Difference Water Index (NDWI) in the delineation
706 of open water features, Int. J. Remote Sens., 17, 1425–1432,
707 https://doi.org/10.1080/01431169608948714, 1996.
708 Oh, J. and Bartos, M.: Scalable, adaptive and risk-informed design of hydrological sensor networks,
709 Nat. Water, 3, 1144–1154, https://doi.org/10.1038/s44221-025-00496-7, 2025.
710 Oki, T. and Kanae, S.: Global hydrological cycles and world water resources, Science, 313, 1068–
711 1072, https://doi.org/10.1126/science.1128845, 2006.
712 Otsu, N.: A threshold selection method from gray-level histograms, IEEE Trans. Syst. Man
713 Cybern., 9, 62–66, https://doi.org/10.1109/TSMC.1979.4310076, 1979.
714 Palmer, M. and Ruhi, A.: Measuring Earth's rivers, Science, 361, 546–547,
715 https://doi.org/10.1126/science.aau3842, 2018.

https://doi.org/10.5194/essd-2026-426
Preprint. Discussion started: 19 June 2026

716 Paris, A., Dias de Paiva, R., Santos da Silva, J., Medeiros Moreira, D., Calmant, S., Garambois,
717 P.-A., Collischonn, W., Bonnet, M.-P., and Seyler, F.: Stage-discharge rating curves based
718 on satellite altimetry and modeled discharge in the Amazon basin, Water Resour. Res., 52,
719 3787–3814, https://doi.org/10.1002/2014WR016618, 2016.
720 Park, C. C.: World-wide variations in hydraulic geometry exponents of stream channels: An
721 analysis and some observations, J. Hydrol., 33, 133–146, https://doi.org/10.1016/0022-
722 1694(77)90103-2, 1977.
723 Patidar, G., Indu, J., and Karmakar, S.: Performance assessment of Surface Water and Ocean
724 Topography (SWOT) mission for WSE measurement across India, Geophys. Res. Lett., 52,
725 e2025GL115804, https://doi.org/10.1029/2025GL115804, 2025.
726 Pavelsky, T. M. and Smith, L. C.: RivWidth: A software tool for the calculation of river widths
727 from remotely sensed imagery, IEEE Geosci. Remote Sens. Lett., 5, 70–73,
728 https://doi.org/10.1109/LGRS.2007.908305, 2008.
729 Pavelsky, T. M.: Using width-based rating curves from spatially discontinuous satellite imagery
730 to monitor river discharge, Hydrol. Process., 28, 3035–3040,
731 https://doi.org/10.1002/hyp.10157, 2014.
732 Resplandy, L., Keeling, R. F., Rödenbeck, C., Stephens, B. B., Khatiwala, S., Rodgers, K. B.,
733 Long, M. C., Bopp, L., and Tans, P. P.: Revision of global carbon fluxes based on a
734 reassessment of oceanic and riverine carbon transport, Nat. Geosci., 11, 504–509,
735 https://doi.org/10.1038/s41561-018-0151-3, 2018.
736 Riggs, R. M., Allen, G. H., Wang, J., Pavelsky, T. M., Gleason, C. J., David, C. H., and Durand,
737 M.: Extending global river gauge records using satellite observations, Environ. Res. Lett., 18,
738 064027, https://doi.org/10.1088/1748-9326/acd407, 2023.
739 Ruhi, A., Messager, M. L., and Olden, J. D.: Tracking the pulse of the Earth's fresh waters, Nat.
740 Sustain., 1, 198–203, https://doi.org/10.1038/s41893-018-0047-7, 2018.
741 Saemian, P., Elmi, O., Stroud, M., Riggs, R., Kitambo, B. M., Papa, F., Allen, G. H., and Tourian,
742 M. J.: Satellite Altimetry-based Extension of global-scale in situ river discharge
743 Measurements (SAEM), Earth Syst. Sci. Data, 17, 2063–2081, https://doi.org/10.5194/essd-
744 17-2063-2025, 2025.

https://doi.org/10.5194/essd-2026-426
Preprint. Discussion started: 19 June 2026

745 Scherer, D., Schwatke, C., Dettmering, D., and Seitz, F.: Monitoring river discharge from space:
746 An optimization approach with uncertainty quantification for small ungauged rivers, Remote
747 Sens. Environ., 315, 114434, https://doi.org/10.1016/j.rse.2024.114434, 2024.
748 Schmidt, A. H., Montgomery, D. R., Huntington, K. W., and Liang, C.: The question of communist
749 land degradation: New evidence from local erosion and basin-wide sediment yield in
750 Southwest China and Southeast Tibet, Ann. Assoc. Am. Geogr., 101, 477–496,
751 https://doi.org/10.1080/00045608.2011.560059, 2011.
752 Sen, P. K.: Estimates of the regression coefficient based on Kendall's tau, J. Am. Stat. Assoc., 63,
753 1379–1389, https://doi.org/10.1080/01621459.1968.10480934, 1968.
754 Sichangi, A. W., Wang, L., Yang, K., Chen, D., Wang, Z., Li, X., Zhou, J., Liu, W., and Kuria, D.:
755 Estimating continental river basin discharges using multiple remote sensing data sets, Remote
756 Sens. Environ., 179, 36–53, https://doi.org/10.1016/j.rse.2016.03.019, 2016.
757 Smith, L. C.: Satellite remote sensing of river inundation area, stage, and discharge: A review,
758 Hydrol. Process., 11, 1427–1439, https://doi.org/10.1002/(SICI)1099-
759 1085(199708)11:10<1427::AID-HYP473>3.0.CO;2-S, 1997.
760 Sun, M., Tangdamrongsub, N., Sun, Y., Dong, J., Sutanudjaja, E., and Smilovic, M.: Assessing
761 and optimizing high-resolution global river streamflow estimates with triple collocation
762 analysis, J. Hydrol., 646, 135122, https://doi.org/10.1016/j.jhydrol.2026.135122, 2026.
763 Syvitski, J. P. M., Vörösmarty, C. J., Kettner, A. J., and Green, P.: Impact of humans on the flux
764 of terrestrial sediment to the global coastal ocean, Science, 308, 376–380,
765 https://doi.org/10.1126/science.1109454, 2005.
766 Tang, G., Clark, M. P., Knoben, W. J. M., Liu, H., Gharari, S., Arnal, L., Beck, H. E., Wood, A.
767 W., Newman, A. J., and Papalexiou, S. M.: The impact of meteorological forcing uncertainty
768 on hydrological modeling: A global analysis of cryosphere basins, Water Resour. Res., 59,
769 e2022WR033767, https://doi.org/10.1029/2022WR033767, 2023.
770 Wang, C., Li, Z., Guyennon, N., Chen, Y., Li, Y., Liang, Q., and Di, Y.: Quantifying the
771 diminished glacier contribution to river runoff in the Tarim Basin, Geophys. Res. Lett., 52,
772 e2025GL114641, https://doi.org/10.1029/2025GL114641, 2025.
773 Wang, K., Liu, X., Cui, P., Zhang, Y., Xie, J., Liu, C., and Gosling, S. N.: China's nationwide
774 streamflow decline driven by landscape changes and human interventions, Sci. Adv., 11,
775 eadu8032, https://doi.org/10.1126/sciadv.adu8032, 2025a.

https://doi.org/10.5194/essd-2026-426
Preprint. Discussion started: 19 June 2026

776 Wang, L., Li, X., Lutz, A., Nepal, S., Chen, D., Yao, T., Su, F., Cuo, L., Yao, Z., Zhang, Y., Hu,
777 Z., Huang, J., Hou, M., Liu, R., Long, J., Chai, C., Liu, Z., Bashir, A., Khanal, S., Sun, H.,
778 Nie, Y., Zhang, Y., and Wang, T.: Acceleration of diverging runoff trends on the Third Pole,
779 Commun. Earth Environ., 6, 907, https://doi.org/10.1038/s43247-025-02854-5, 2025b.
780 Wang, Y. and Li, Y.: China Daily River Discharge Records (CDR²) dataset [Data set], Zenodo,
781 https://doi.org/10.5281/zenodo.20152832, 2026.
782 Xu, H.: Modification of normalised difference water index (NDWI) to enhance open water features
783 in remotely sensed imagery, Int. J. Remote Sens., 27, 3025–3033,
784 https://doi.org/10.1080/01431160600589179, 2006.
785 Yang, L., Zhao, G., Tian, P., Mu, X., Tian, X., Feng, J., and Bai, Y.: Runoff changes in the major
786 river basins of China and their responses to potential driving forces, J. Hydrol., 607, 127536,
787 https://doi.org/10.1016/j.jhydrol.2022.127536, 2022.
788 Yang, X., Pavelsky, T. M., Allen, G. H., and Donchyts, G.: RivWidthCloud: An automated Google
789 Earth Engine algorithm for river width extraction from remotely sensed imagery, IEEE
790 Geosci. Remote Sens. Lett., 17, 217–221, https://doi.org/10.1109/LGRS.2019.2920225, 2019.
791 Yao, T., Bolch, T., Chen, D., Gao, J., Immerzeel, W., Piao, S., Su, F., Thompson, L., Wada, Y.,
792 Wang, L., Wang, T., Wu, G., Xu, B., Yang, W., Zhang, G., and Zhao, P.: The imbalance of
793 the Asian water tower, Nat. Rev. Earth Environ., 3, 618–632, https://doi.org/10.1038/s43017-
794 022-00299-4, 2022.
795 Yuan, Z., Lin, P., Guo, X., Zhang, K., and Beck, H. E.: Revisiting at-a-station hydraulic geometry
796 using discharge observations and satellite-derived river widths, J. Remote Sens., 4, 0271,
797 https://doi.org/10.34133/remotesensing.0271, 2024.
798 Zheng, H., Yang, Z.-L., Lin, P., Wei, J., Wu, W.-Y., Li, L., Zhao, L., and Wang, S.: On the
799 sensitivity of the precipitation partitioning into evapotranspiration and runoff in land surface
800 parameterizations, Water Resour. Res., 55, 95–111, https://doi.org/10.1029/2017WR022236,
801 2019.